

Charged Higgs-boson production in association with an electron and a neutrino at electron–positron colliders

OLIVER BREIN¹ and TERRANCE FIGY²

Institute for Particle Physics Phenomenology,
University of Durham, DH1 3LE, Durham, United Kingdom

Abstract

We present results of a calculation of the cross section for the production of a charged Higgs boson in association with an electron and a neutrino at electron–positron colliders ($e^+e^- \rightarrow H^+e^-\bar{\nu}_e, H^-e^+\nu_e$). We study predictions for the cross section in the Minimal Supersymmetric Standard Model (MSSM) and the Two Higgs Doublet Model (THDM), highlighting possible differences. The process is effectively loop-induced in both models. Hence, the cross section is expected to be strongly model-dependent. Most notably, due to the presence of superpartners, the MSSM amplitude contains Feynman graphs of pentagon-type, which are not present in the THDM. This is the first complete one-loop calculation of the cross section for this process in the THDM and the MSSM. For both models, so far, only approximate results with limited ranges of validity were available. Our main aim here is to clarify several open questions in the existing literature on this process. Specifically, we will discuss the validity of the Heavy Fermion loop approximation in both models, and of the Fermion/Sfermion loop approximation in the MSSM.

¹E-mail: Oliver.Brein@durham.ac.uk

²E-mail: Terrance.Figy@durham.ac.uk

1 Introduction

The detection of a charged Higgs boson would be an unambiguous sign of an extended Higgs sector. With only one Higgs doublet, like in the Standard Model, all charged scalar degrees of freedom present are needed to provide the longitudinal degrees of freedom of the charged electroweak bosons W^\pm .

The search for charged Higgs bosons proceeds currently at the Tevatron and will be taken up by the LHC experiments in the near future. For the Tevatron the only significant production mode of charged Higgs bosons is from the decay of top quarks in $t\bar{t}$ production events. In the presently unprobed range of charged Higgs mass values, m_{H^\pm} , above the LEP limit of about 80 GeV [1], this is the only relevant channel which can be reached with significant statistics given the luminosity and collision energy of the protons and anti-protons at the Tevatron. The observability of this channel relies on the values of the Yukawa couplings of the charged Higgs boson to top and bottom quarks and to $\tau\nu_\tau$. The former determines the production rate, while the latter enters the branching ratios for the decays $H^\pm \rightarrow \tau\nu_\tau$. Overproduction of τ leptons compared to the SM expectation is the primary signature of charged Higgs bosons. The best H^\pm search channels at hadron colliders identified so far, depend on Yukawa interactions of heavy quarks. Furthermore, in Two-Higgs-Doublet-Models, the H^\pm Yukawa couplings depend strongly on the ratio of the vacuum expectation values $v_2/v_1 \equiv \tan\beta$ of the two Higgs-doublets. Therefore, the discovery reach for a charged Higgs boson at hadron colliders in such models also depends strongly on the value of $\tan\beta$. For instance, in the Type-II THDM and the MSSM, the mass reach in the intermediate $\tan\beta$ -region around $\tan\beta = 15$ is rather low compared to the high- and low- $\tan\beta$ region, even at the LHC.

With an electron-positron collider, the detection of a charged Higgs boson is rather straightforward if its energy allows for H^+H^- pair production. As the tree-level amplitude for this process consists of s -channel photon and Z -boson exchange, the production cross section is essentially independent of other parameters of the model the charged Higgs boson is embedded in. Furthermore, for m_{H^\pm} above the top-bottom threshold, the dominant decay mode $H^\pm \rightarrow tb$ can be utilised to search for charged Higgs bosons [2], unlike at hadron colliders where processes with these decay modes are swamped by background events. The mass-reach of the pair production process as a search channel at an electron positron collider is essentially independent of $\tan\beta$ and only limited by the available collision energy \sqrt{s} .

It is a topic of current research to explore the mass-reach of a future electron positron collider for charged Higgs bosons beyond the pair production limit of about $\sqrt{s}/2$. Single production of one charged Higgs boson in association with one or a few particles with an overall mass less than m_{H^\pm} can proceed via several channels. Unfortunately, the electroweak gauge bosons as intermediate particles normally do not lead to tree-level processes similar to Higgs-strahlung or vector-boson fusion for neutral Higgs boson production. The reason is that the $ZW^\pm H^\mp$ interaction is absent in any Higgs sector model with multiple doublets and restricted to have a quite small coupling constant in many other models because of the measured electroweak ρ -parameter [3].

The only relevant single charged Higgs boson production process with only two particles in the final state is the (effectively) loop-induced $W^\pm H^\mp$ production which has been studied in detail in the general THDM and the MSSM [4, 5, 6]. Relevant processes with a tree-level amplitude start with three particles in the final-state. Among those, the final states $H^\pm tb$ [7, 8] and $H^\pm \tau \nu_\tau$ [8, 9] appear to be the most promising.

The loop-induced process $e^+e^- \rightarrow H^-e^+\nu_e$ (and its charge conjugate) have also been suggested as potential charged Higgs boson discovery processes. Unlike in charged Higgs boson production together with tb or $\tau\nu_\tau$, this process has t -channel Feynman graphs, similar to the vector boson fusion process in the SM, which grows like $\log(s/m_{H^\pm}^2)$ for $s \gg m_{H^\pm}^2$. The cross section for this process has been calculated in various approximations. For the calculation of the THDM cross section in Ref. [8] only the t -channel Feynman graphs have been considered with insertions of effective vertices for the loop-induced $\gamma W^\pm H^\mp$ and $ZW^\pm H^\mp$ interaction. Among the contributions to those one-loop vertices, bosonic contributions, i.e. contributions from virtual Higgs, Goldstone and gauge bosons, have been checked to be small in the region where the vertex interactions are substantial and then neglected in the numerical evaluation in [8]. In Ref. [10] the THDM cross section is calculated taking all terms quadratic in the $H^\pm tb$ Yukawa couplings into account. This amounts to taking all one-loop Feynman graphs with top and bottom quarks into account and neglecting all bosonic contributions. Thus, in this study the s -channel contributions have been included in the top–bottom loop approximation. In Ref. [11] preliminary results have been reported on an evaluation of the MSSM cross section using the approximation of only taking fermion and sfermion loops into account. In this calculation, also all contributions from virtual gauge and Higgs bosons have been neglected. Furthermore, all other contributions from virtual superpartners which do not contain a closed sfermion loop have been neglected as well.

The current state of research concerning the process $e^+e^- \rightarrow H^-e^+\nu_e + (\text{c.c.})$ leaves quite a few open questions which we would like to address in this paper. First, neglecting the bosonic contributions was justified in [8, 10] by their reported smallness in the loop-induced $\gamma W^\pm H^\mp$ and $ZW^\pm H^\mp$ interactions [5]. Yet, in the process at hand there are also bosonic four-point loop graphs in the THDM, which have never been computed in this context. Naturally, the MSSM also has additional four-point loops with virtual superpartners and, furthermore, even five-point (“pentagon”) superpartner loops. Specifically, there are triangle-, box- and pentagon-type loops involving neutralinos, gauginos and first generation sleptons.

The rest of the paper is organized as follows. In Section 2 we present the essential process kinematics, a complete list of Feynman graphs for the process in the MSSM and the THDM, and a description of the approximations which have been used so far in previous calculations of this process. Section 3 contains numerical results for the total cross section of $e^+e^- \rightarrow H^-e^+\nu_e + (\text{c.c.})$ for two interesting MSSM sample scenarios. In this section, we demonstrate when certain approximations describe the complete MSSM result reasonably well and when (and how badly) they fail to do so. Our conclusions follow in Section 4.

2 $e^+e^- \rightarrow H^-e^+\nu_e$ in the MSSM and THDM

2.1 Kinematics

We study the reaction

$$e^+(k, \lambda) + e^-(q, \bar{\lambda}) \rightarrow H^-(p) + e^+(k', \lambda') + \nu_e(q'),$$

where k and q denote the momenta of the initial-state positron and electron, q' and k' the momenta of the final-state neutrino and positron, and p the momentum of the final-state Higgs boson H^- . Additionally, the electron and the positrons, are characterized by their spin polarization $\lambda, \bar{\lambda}, \lambda' (= \pm \frac{1}{2})$.

The total unpolarized cross section can be written as an integral over a 4-fold differential cross section [12]:

$$\sigma = \frac{1}{4} \sum_{\lambda, \bar{\lambda}, \lambda' = \pm 1/2} \int_{m_e}^{k'^0_{\max}} dk'^0 \int_{p^0_{\min}}^{p^0_{\max}} dp^0 \int_{\cos \theta_{\min}}^{\cos \theta_{\max}} d \cos \theta \int_0^{2\pi} d\eta \frac{d^4 \sigma_{\lambda \bar{\lambda} \lambda'}}{dk'^0 dp^0 d \cos \theta d\eta}, \quad (1)$$

with

$$k'^0_{\max} = \frac{s - m_{H^\pm}^2 + m_e^2}{2\sqrt{s}}, \quad p^0_{\max, \min} = (\sqrt{s} - k'^0) \frac{1 + \xi}{2} \pm |\vec{k}'| \frac{1 - \xi}{2},$$

$$\xi = \frac{m_{H^\pm}^2}{s - 2\sqrt{s} k'^0 + m_e^2}, \quad \cos \theta_{\max, \min} = \pm 1 \mp \delta \cos \theta_{\text{cut}}.$$

The differential cross section is related to the squared matrix element $|\mathcal{M}_{\lambda \bar{\lambda} \lambda'}|^2$ through

$$\frac{d^4 \sigma_{\lambda \bar{\lambda} \lambda'}}{dk'^0 dp^0 d \cos \theta d\eta} = \frac{|\mathcal{M}_{\lambda \bar{\lambda} \lambda'}|^2}{(4\pi)^4 s \sqrt{1 - 4m_e^2/s}}. \quad (2)$$

The angle between the three-momentum of the in- and outgoing positron, θ is defined by

$$\cos \theta = \frac{\vec{k}' \cdot \vec{k}}{|\vec{k}'| |\vec{k}|}, \quad (3)$$

and η is the angle between the plane spanned by the three-momenta of the three final-state particles and a plane perpendicular to the beam axis.

In order to have a realistic scenario concerning the detectability of the outgoing positron, we employ an angular cut-off $\delta \cos \theta_{\text{cut}} = 10^{-3}$. This cuts off all final state positrons which scatter with an angle less than 44.7 mrad to the beam axis. This choice is inspired by the TESLA Detector Technical Design Report [13] where a detection of electrons and positrons down to 4.6 mrad is foreseen, but with angles below 30 mrad only used for luminosity monitoring.

2.2 Feynman graphs

In the MSSM and THDM the tree-level amplitude for the process under study contains the $H^-e^+\nu_e$ Yukawa coupling, which is $\propto m_e/m_W \approx 6 \cdot 10^{-6}$. Thus, the tree-level contribution is strongly suppressed and can be neglected. The process can be called effectively loop-induced. In our calculation we take into account all one-loop contributions to the amplitude which do not vanish in the limit $m_e = 0$. For this reason, Feynman graphs with an insertion of an s -channel $Z - A$ mixing self-energy, or a t -channel neutrino self-energy, and the radiative corrections to $e^+e^-\{h^0, H^0, A^0\}$ Yukawa couplings and large parts to the $e^\pm\nu_e H^\mp$ Yukawa coupling need not be considered. In the MSSM, there is a contribution to the $e^\pm\nu_e H^\mp$ Yukawa coupling which involves virtual charginos or neutralinos which is finite and does not vanish for $m_e = 0$. Those contributions are taken into account in our calculation.

The Feynman graphs of the MSSM loop contributions can be divided into

- graphs with $W^- - H^-$ and $G^- - H^-$ mixing self-energies on the external H^- line (see Fig.1),
- graphs with the loop-induced $\gamma W^+ H^-$ or $Z W^+ H^-$ vertex (see Fig.1),
- graphs with the non-vanishing part of the $e^+\nu_e H^-$ vertex (see Fig.2),
- box-type graphs (see Figs. 3 and 4),
- pentagon-type graphs (see Fig.5).

The self-energy and vertex insertions depicted in Fig.1 consist of closed loops of fermions and sfermions, loops with gauge and Higgs bosons, and loops with electroweak gauginos and sfermions.³

In the literature there have been several approximations adopted to simplify the calculations as a complete calculation in the MSSM requires the calculation of pentagon graphs. Below, we define the typical approximations and to what subset of Feynman graphs they correspond to.

Fermion/Sfermion Approximation : Only closed loops with fermions or sfermions are included in the calculation. For the THDM part of the amplitude this approximation means neglecting all bosonic loops. The superpartner part of the amplitude comprises the set of graphs analogous to the fermion loop amplitudes, with fermions replaced by sfermions plus some additional related ones involving 4-point interactions with sfermions. Such an approximation can be justified in scenarios where the masses of the third-generation sfermions (especially squarks) lie well below the masses of slepton and electroweak gaugino masses which appear in all the neglected graphs (see Figs. 2, 4 and 5) and provide additional mass suppression factors.

³The Feynman graphs for these insertions can be found e.g. in [6].

sTHDM : No superpartner graphs are included in the calculation. This subset of graphs corresponds to the full THDM with the Higgs sector parameters chosen according to the corresponding MSSM scenario. It is usually a useful approximation to the full MSSM result in parameter scenarios where all superpartners are rather heavy compared to the SM particles.

Heavy Fermion Approximation : Only the loops with third generation fermions are taken into account. This approximation consists of all THDM terms proportional to the usually dominant third generation Yukawa couplings and neglects the bosonic loops of Fig. 3. In the literature, this approximation is usually further simplified by only taking the loops with top and bottom quarks into account. In the present calculation, we also include the loops involving tau leptons which has a small but noticeable effect on the results.

2.3 Calculation

Although the tree-level contribution vanishes in the limit of vanishing electron mass, which we consider, the need for renormalization arises at one-loop. In the gauge and Higgs boson sector there are divergent off-diagonal propagator entries leading to H^\pm - W^\pm and H^\pm - G^\pm mixing and, connected to this, the one-loop $\gamma W^\pm H^\mp$ and $ZW^\pm H^\mp$ vertex functions are divergent too (see Fig. 1). We use the on-shell renormalization scheme of Ref. [14], the application of which to the present situation is discussed e.g. in [4, 5, 6]. In this scheme the renormalization conditions relevant to our calculation are the following.

- Renormalized tadpole graphs for the neutral CP-even Higgs bosons, h^0, H^0 , vanish:

$$\hat{t}_{h^0} = t_{h^0} + \delta t_{h^0} = 0, \quad (4)$$

$$\hat{t}_{H^0} = t_{H^0} + \delta t_{H^0} = 0. \quad (5)$$

This guarantees that the parameters v_1, v_2 in the renormalized Lagrangian describe the minimum of the Higgs potential at one-loop order.

- Physical charged Higgs bosons H^\pm do not mix with longitudinally polarized W^\pm bosons, i.e. the real part of the renormalized H^\pm - W^\mp mixing self-energy⁴,

$$\hat{\Sigma}_{HW}(k^2) = \Sigma_{HW}(k^2) - m_W^2 \delta Z_{HW}, \quad (6)$$

vanishes if the momentum k of H^\pm is on mass-shell:

$$\text{Re } \hat{\Sigma}_{HW}(k^2) \Big|_{k^2=m_{H^\pm}^2} = 0. \quad (7)$$

⁴ The renormalized H^\pm - W^\pm mixing self-energy is defined as the coefficient of $-i\frac{k^\mu}{m_W}$ of the amputated renormalized H^\pm - W^\pm propagator.

Conditions (4) and (5) amount to neglecting all Feynman graphs with tadpoles in our calculation. The specific expressions for the tadpole counter-terms are not needed here. Condition (7) fixes the renormalization constant δZ_{HW} :

$$\delta Z_{HW} = \frac{1}{m_W^2} \text{Re} \Sigma_{HW}(m_{H^\pm}^2). \quad (8)$$

Furthermore, the renormalization of the divergent H^\pm - G^\pm mixing self-energy is connected to the H^\pm - W^\pm mixing self-energy through a Slavnov–Taylor identity [15]:

$$k^2 \hat{\Sigma}_{HW}(k^2) - m_W^2 \hat{\Sigma}_{HG}(k^2) = 0. \quad (9)$$

As a consequence, the real part of the renormalized H^\pm - G^\pm mixing self-energy,

$$\hat{\Sigma}_{HG}(k^2) = \Sigma_{HG}(k^2) - k^2 \delta Z_{HG}, \quad (10)$$

also vanishes for $k^2 = m_{H^\pm}^2$:

$$\text{Re} \hat{\Sigma}_{HG}(k^2) \Big|_{k^2=m_{H^\pm}^2} = 0, \quad (11)$$

and fixes the renormalization constant δZ_{HG} :

$$\delta Z_{HG} = -\text{Re} \Sigma_{HG}(m_{H^\pm}^2)/m_{H^\pm}^2. \quad (12)$$

The Feynman rules for the corresponding counter-term interactions read:

$$\Gamma_{\text{CT}}[H^\mp W^\pm(k^\mu)] = i \frac{k^\mu}{m_W} m_W^2 \delta Z_{HW}, \quad (13)$$

$$\Gamma_{\text{CT}}[\gamma_\mu W_\nu^\pm H^\mp] = -ie m_W g_{\mu\nu} \delta Z_{HW}, \quad (14)$$

$$\Gamma_{\text{CT}}[Z_\mu W_\nu^\pm H^\mp] = ie m_W \frac{s_w}{c_w} g_{\mu\nu} \delta Z_{HW}, \quad (15)$$

$$\Gamma_{\text{CT}}[H^\mp G^\pm(k)] = ik^2 \delta Z_{HG}, \quad (16)$$

where Z, W^\pm and γ denote the electroweak gauge bosons and the photon, and k^μ the momentum of the W^\pm boson, chosen as incoming.

The calculation of the amplitude has been performed using the 't Hooft–Feynman gauge and Constrained Differential Renormalization [16] with the help of the computer programs FeynArts 3.2 and FormCalc 5.1 [12]. In particular, we made use of the numerical routines for the evaluation of the 5-point loop-integrals implemented in LoopTools 2.2 [17] employing the methods of [18]. For our purpose, we extended the existing FeynArts model file for the MSSM by including the necessary counter-term definitions and Feynman rules for the counter-term interactions.

A subclass of Feynman graphs corresponds to the production of a charged Higgs boson H^- in association with a virtual W^+ and its subsequent decay into $e^+ \nu_e$. Those graphs can become resonant which requires to take the width of the W -boson into account. We have chosen the finite width scheme and have introduced a constant finite width Γ_W by replacing in the 't Hooft-Feynman gauge:

$$\frac{-ig^{\mu\nu}}{p^2 - m_W^2} \rightarrow \frac{-ig^{\mu\nu}}{p^2 - m_W^2 + im_W \Gamma_W}.$$

3 Results

3.1 Parameter scenarios

We pick the MSSM parameter scenarios from [6] which are partly modifications from the LEP Higgs search benchmark scenarios [19]: the m_h^{\max} scenario with a lower sfermion mass scale and the small- α_{eff} scenario. This will allow us to re-use parts of the discussion of the behaviour of $\sigma(e^+e^- \rightarrow W^\pm H^\mp)$ in those scenarios from [6]. The two MSSM parameter scenarios are specified as follows:

$m_h^{\max}(400)$ scenario: The soft-breaking sfermion mass parameter is set to $M_{\tilde{f}} = 400$ GeV. The off-diagonal term $X_t (= A_t - \mu \cot \beta)$ in the top-squark mass matrix is set to $2M_{\tilde{f}}$ ($= 800$ GeV). The Higgsino and gaugino mass parameters have the settings $\mu = -200$ GeV, $M_1 = M_2 = 200$ GeV, $M_{\tilde{g}} = 800$ GeV. When $\tan \beta$ is changed, A_t is changed accordingly to ensure $X_t = 2M_{\tilde{f}}$. The settings of the other soft-breaking scalar-quark Higgs couplings are $A_b = A_t$ and $A_f = 0$ ($f = e, \mu, \tau, u, d, c, s$).

small- α_{eff} scenario: This scenario gives rise to suppressed branching ratios for the decays $h^0 \rightarrow b\bar{b}$ and $\tau^+\tau^-$, especially for large $\tan \beta$ and moderate values of m_A . The settings are: $M_{\tilde{f}} = 800$ GeV, $X_t = -1100$ GeV, $M_1 = M_2 = 500$ GeV, $\mu = 2000$ GeV. Also here, A_t is changed if $\tan \beta$ changes in order to keep the value of X_t fixed, $A_b = A_t$ and $A_f = 0$ ($f = e, \mu, \tau, u, d, c, s$).

The resulting masses of the Higgs bosons and the relevant superpartner particles for these parameter choices are given in Table 1.

3.2 Cross sections

We present results for the cross section of the process $e^+e^- \rightarrow (H^+e^-\bar{\nu}_e, H^-e^+\nu_e)$ assuming unpolarized beams⁵ and a collider energy of 1 TeV. Assuming the collider would accumulate 1000 events/fb of integrated luminosity, a cross section of 0.05 fb would result in 50 expected events. This can be taken as a reasonable lower limit for the observability of a particular discovery channel and is often not reached in our sample scenarios. However, our aim here is not primarily phenomenology but to clarify the relationship between different commonly used approximations and the complete MSSM result. Specifically, we show cross section results for the $m_h^{\max}(400)$ scenario (Figs. 6a, 6c, 7a, 7c) and the small- α_{eff} scenario (Figs. 6b, 6d, 7b, 7d) and demonstrate when certain approximations describe the complete result reasonably well and when (and how badly) they fail to do so.

⁵ From the analysis of the related process $e^+e^- \rightarrow H^\pm W^\mp$ [6], we expect that the cross section can be up to a factor of 4 higher than in the unpolarized case, if optimal polarization of the e^- and e^+ beams is assumed.

	$m_h^{\max}(400)$ scenario		small- α_{eff} scenario	
	$\tan\beta = 5$	$\tan\beta = 30$	$\tan\beta = 5$	$\tan\beta = 30$
Higgs masses for $m_{H^\pm} = 250$ [500] GeV				
m_{h^0} [GeV]	115.5 [116.9]	122.1 [122.0]	113.6 [113.9]	119.9 [119.2]
m_{H^0} [GeV]	240.7 [494.7]	232.3 [491.3]	237.2 [493.1]	234.0 [492.1]
m_{A^0} [GeV]	237.1 [493.5]	232.6 [492.2]	238.9 [494.4]	238.3 [494.4]
Stau, sbottom and stop masses				
$m_{\tilde{\tau}_1}$ [GeV]	398.5	387.3	789.2	730.5
$m_{\tilde{\tau}_2}$ [GeV]	406.3	417.3	813.0	866.3
$m_{\tilde{b}_1}$ [GeV]	391.9	360.7	769.2	596.0
$m_{\tilde{b}_2}$ [GeV]	412.7	440.5	832.0	963.8
$m_{\tilde{t}_1}$ [GeV]	224.4	224.0	692.0	691.9
$m_{\tilde{t}_2}$ [GeV]	569.7	569.6	925.2	925.1
Chargino and neutralino masses				
$m_{\chi_1^\pm}$ [GeV]	166.3	153.5	497.8	498.9
$m_{\chi_2^\pm}$ [GeV]	255.5	263.4	2003.8	2003.5
$m_{\chi_1^0}$ [GeV]	93.9	89.8	236.8	237.1
$m_{\chi_2^0}$ [GeV]	163.8	154.9	497.8	498.9
$m_{\chi_3^0}$ [GeV]	215.1	211.9	2001.1	2001.6
$m_{\chi_4^0}$ [GeV]	252.4	262.1	2003.7	2002.9

Table 1: Masses of the Higgs bosons, the most $\tan\beta$ -sensitive sfermions, charginos and neutralinos for the two sample scenarios and different values of $\tan\beta$ and m_{H^\pm} . All other sfermion masses are equal to $M_{\tilde{f}}$ within $\pm 2\%$.

3.2.1 $m_h^{\max}(400)$ scenario

The $m_h^{\max}(400)$ scenario has rather light squarks, neutralinos and charginos compared to the assumed collider energy of 1 TeV. Therefore, all these particles can contribute significantly to the amplitude of the process. Especially, there are enhanced couplings of third-generation squarks to the charged Higgs bosons.

In Fig. 6a, we show the integrated cross section as a function of charged Higgs mass, m_{H^\pm} , for $\tan\beta = 30$. Depending on m_{H^\pm} , the cross section prediction of the full MSSM (solid line) can be up to two orders of magnitude larger than of the sTHDM (dotted line). For rather large m_{H^\pm} , between 550 GeV and 750 GeV, the cross section experiences threshold enhancement basically through stop–sbottom loop graphs, which dominate the amplitude in this region, as has been noted for the related process $e^+e^- \rightarrow W^\pm H^\mp$ in [6]. Naturally, in this region, the Fermion/Sfermion approximation used in [11] comes quite close to the full MSSM prediction. For m_{H^\pm} below 550 GeV this approximation ceases to be a good approximation to the full MSSM. Away from the region where the loop graphs with stops and sbottoms dominate, the ones with neutralinos and charginos

become relevant as well and lead to a cross section more than twice as large as in the Fermion/Sfermion approximation.

The Heavy Fermion approximation works well as an approximation to the sTHDM for m_{H^\pm} above the threshold $m_{H^\pm} = m_t + m_b$ in top–bottom loops up to about 500 GeV where the full sTHDM amplitude starts to experience enhancement from box-type Feynman graphs which consist of loops with virtual gauge and Higgs bosons (see Fig 3). Around the peak of this effect, at $m_{H^\pm} \approx 640$ GeV, the full sTHDM result lies almost a factor of two above the Heavy Fermion approximation. But also for low m_{H^\pm} ($\lesssim 150$ GeV), the result in the full sTHDM is about 15% larger than in the Heavy Fermion approximation.

In Fig. 6c, we show the integrated cross section as a function of charged Higgs mass, m_{H^\pm} , for $\tan\beta = 5$. For small $\tan\beta$ the difference between the full MSSM and the Fermion/Sfermion approximation becomes less dramatic than in the high- $\tan\beta$ case. However, there is, for all displayed m_{H^\pm} , a clear difference between the two results, the full MSSM lying between -13% to -50% below the approximation. The sTHDM result agrees perfectly with the Heavy Fermion approximation and both agree quite good with the Fermion/Sfermion approximation, except for m_{H^\pm} between 600 and 700 GeV, which is the region of stop–sbottom thresholds. Unlike in the high $\tan\beta$ case, there is no peak but a dip, which is also quite similar to the findings for $e^+e^- \rightarrow H^\pm W^\mp$ [6].

The Figures 7a and 7c show the $\tan\beta$ dependence of the cross section for $m_{H^\pm} = 250$ GeV and 500 GeV respectively. The case $m_{H^\pm} = 250$ GeV is particularly interesting, as it lies exactly in the area of Fig. 6a where even the pentagon-type graphs make a noticeable contribution to the amplitude. We see again that the Fermion/Sfermion approximation does not describe the full MSSM well. For $m_{H^\pm} = 250$ [500] GeV it deviates by about $+30\%$ [40%] for small $\tan\beta$ and -50% [-23%] for large $\tan\beta$. The Heavy Fermion approximation comes quite close to the full sTHDM result, except for the large $\tan\beta$ region for $m_{H^\pm} = 500$ GeV which is where the box amplitudes become enhanced as noted above. However, there is no place in the displayed scenarios where the Heavy Fermion approximation is a reasonable approximation to the full MSSM, except for very small $\tan\beta$ (say $\tan\beta < 2$) and, accidentally, at a cross-over point around $\tan\beta = 10$.

3.2.2 small- α_{eff} scenario

In the small- α_{eff} scenario, all the sfermion thresholds in the amplitude lie well above 1 TeV and the lowest chargino–neutralino threshold lies above 700 GeV. Hence, the superpartner effects in this scenario are a bit milder than in the previous one. However, once the mass scale m_{H^\pm} approaches the level of the sfermion mass scales, stop–sbottom loop graphs can still lead to large effects if $\tan\beta$ is large.

In Figures 6b and 6d we show the integrated cross section as a function of m_{H^\pm} for $\tan\beta = 30$ and 5, respectively. For large $\tan\beta$ (see Fig. 6b) there is no point where the Heavy Fermion approximation is a good approximation to the full MSSM result. This can only be possible for scenarios with a superpartner mass scale considerably higher than 800 GeV. However, for the most part the Fermion/Sfermion approximation works reasonably well to describe the full MSSM and the Heavy Fermion approximation likewise

to describe the full THDM. An exception is the low charged Higgs mass region around $m_{H^\pm} \lesssim 300$ GeV where the gauge and Higgs boson loops, which are neglected in both approximations (i.e. also in all previous calculations of this process), contribute significantly, raising the full MSSM and sTHDM result by up to $\approx 50\%$ compared to their approximations. For small $\tan\beta$ (see Fig. 6d) the Fermion/Sfermion approximation reproduces the full MSSM result over the whole displayed range within at most $\pm 10\%$ and the agreement between the Heavy Fermion approximation and the sTHDM is similar. Yet, the MSSM result is usually larger than the sTHDM result, up to about 30%.

The $\tan\beta$ dependence of the cross section, shown in Figs. 7b and 7d for $m_{H^\pm} = 250$ GeV and 500 GeV respectively, merely underline the statements above.

3.2.3 The pentagon contribution

So far, not many MSSM processes which include pentagon-type Feynman graphs of superpartners have been studied. Therefore, a closer look at this part of the amplitude seems to be on order. Although the main contribution of the pentagon graphs to the cross section of the full MSSM comes from the interference of those graphs with the remainder of the MSSM amplitude, we will study here the cross section obtained from squaring the pentagon graphs alone for clarity.

In Fig. 8a we show this cross section as a function of m_{H^\pm} for all the parameter scenarios we studied above. For $\tan\beta = 30$ in the $m_h^{\max}(400)$ scenario we see threshold peaks for $m_{H^\pm} \approx m_{\chi_i^\pm} + m_{\chi_j^0}$ for some but not all combinations of i and j , depending on the couplings and mixing matrices of the charginos and neutralinos. For m_{H^\pm} in the vicinity of the lowest threshold, $m_{\chi_1^\pm} + m_{\chi_1^0} = 243.3$ GeV, one even gets a noticeable contribution to the full result. In the small- α_{eff} scenario the same threshold lies around 740 GeV (see Fig. 8a), but in this case the pentagon contribution is way too small to influence the numerical value of the cross section significantly.

The $\tan\beta$ dependence of the ‘‘pentagon-only’’ cross section is displayed in Fig. 8b. The case of $m_{H^\pm} = 250$ GeV in the $m_h^{\max}(400)$ scenario shows the most interesting behaviour. The cross section rises by more than an order of magnitude with $\tan\beta$ going through a peak around $\tan\beta = 10$. The reason for this is, that the neutralino and chargino masses depend slightly on $\tan\beta$ and the sum $m_{\chi_1^\pm} + m_{\chi_1^0}$ passes through the value 250 GeV around $\tan\beta = 10$. The value of $m_{\chi_1^\pm} + m_{\chi_1^0}$ changes quickly for small $\tan\beta$ and reaches a plateau value close to 250 GeV for high $\tan\beta$. This is why the cross section reaches a plateau for high $\tan\beta$ as well.

In our sample scenarios, the MSSM is usually well approximated by neglecting the pentagon graphs, except for the threshold enhancement situations mentioned above. In MSSM scenarios with higher masses for the charginos, neutralinos and sleptons than in our sample scenarios, with no thresholds within the reach of the collider, this statement should hold without exception.

Neglecting the pentagon graphs in such scenarios is then also quite time saving from a computational point of view. The inclusion of the pentagons graphs adds 1216 distinct 5-point integrals to the amplitude to be calculated and the evaluation of those uses the

reduction of each 5-point integral to five 4-point integrals. This has to be contrasted to only 52 distinct 4-point integrals to be calculated for the amplitude without pentagons.

4 Conclusions

We have presented the first complete one-loop calculation of the process $e^+e^- \rightarrow H^-e^+\nu_e + (\text{c.c.})$ in both the THDM and MSSM. We have examined the differences that arise in using the various approximations which have been used in calculations of this process previously as outlined in Section 2.2. We find that in the small- α_{eff} scenario, that cross sections computed in the Fermion/Sfermion approximation are comparable to those computed in the full MSSM while cross sections computed in the Heavy Fermion approximation are comparable to those computed in the full THDM. However, these approximations simply fail for the $m_h^{\text{max}}(400)$ scenario. The reason is that in this scenario the virtual particles in the loops have lower masses which is why their contribution to the amplitude cannot be neglected. We further point out that cross sections computed in the Heavy Fermion approximation for both scenarios usually disagree completely with cross sections computed in the MSSM, except for very low $\tan\beta$.

For our sample scenarios we explicitly show that the pentagon graphs in the MSSM usually contribute negligibly to the total cross section. The MSSM is well approximated in the small- α_{eff} scenario by neglecting the pentagon graphs. This is also true for the $m_h^{\text{max}}(400)$ scenario except in threshold regions.

Acknowledgements

Work supported in part by the European Community's Marie-Curie Research Training Network under contract MRTN-CT-2006-035505 'Tools and Precision Calculations for Physics Discoveries at Colliders'.

References

- [1] W. M. Yao *et al.* [Particle Data Group], J. Phys. G **33** (2006) 1.
- [2] M. Battaglia, A. Ferrari, A. Kiiskinen and T. Maki, in N. Graf (ed.), *Proc. of the APS/DPF/DPB Summer Study on the Future of Particle Physics (Snowmass 2001)*, hep-ex/0112015.
- [3] J. A. Grifols and A. Mendez, Phys. Rev. D **22** (1980) 1725.
- [4] H.E. Logan, S. Su, Phys. Rev. D **66** (2002) 035001 and Phys. Rev. D **67** (2003) 017703; S. H. Zhu, hep-ph/9901221; A. Arhrib, M. Capdequi Peyranere, W. Hollik, G. Moutaka, Nucl. Phys. B **581** (2000) 34; O. Brein, in: *Proceedings of the 10th*

International Conference On Supersymmetry And Unification Of Fundamental Interactions (SUSY02), DESY Hamburg 2002, hep-ph/0209124.

- [5] S. Kanemura, Eur. Phys. J. C **17** (2000) 473;
- [6] O. Brein and T. Hahn, Eur. Phys. J. **52** (2007) 397, hep-ph/0610079.
- [7] A. Djouadi, J. Kalinowski and P. M. Zerwas, Z. Phys. C **54** (1992) 255;
B. A. Kniehl, F. Madricardo and M. Steinhauser, Phys. Rev. D **66** (2002) 054016.
- [8] S. Kanemura, S. Moretti and K. Odagiri, JHEP **0102** (2001) 011.
- [9] A. Gutierrez-Rodriguez and O. A. Sampayo, Phys. Rev. D **62** (2000) 055004 and
Rev. Mex. Fis. **48** (2002) 413.
- [10] T. Farris, H. E. Logan and S. f. Su, Phys. Rev. D **69** (2004) 035005.
- [11] O. Brein, T. Hahn, S. Heinemeyer, G. Weiglein, in: *Proceedings of the 10th International Conference On Supersymmetry An Unification Of Fundamental Interactions (SUSY02)*, DESY Hamburg 2002, hep-ph/0402053.
- [12] J. Küblbeck, M. Böhm, A. Denner, Comput. Phys. Commun. **60** (1990) 165; H. Eck,
Ph.D. thesis, University of Würzburg (1995); T. Hahn, Comput. Phys. Commun.
140 (2001) 418; T. Hahn and C. Schappacher, Comput. Phys. Commun. **143** (2002)
54
- [13] T. Behnke, S. Bertolucci, R. D. Heuer and R. Settles (eds.), TESLA Technical
design report, Part 4, Report-No. ECFA-2001-209.
- [14] M. Böhm, W. Hollik, H. Spiesberger, Fortsch. Phys. **34** (1986) 687;
P. H. Chankowski, S. Pokorski and J. Rosiek, Nucl. Phys. B **423** (1994) 437;
A. Dabelstein, Z. Phys. C **67** (1995) 495.
- [15] J. A. Coarasa, D. Garcia, J. Guasch, R. A. Jimenez, J. Sola, Eur. Phys. J. C **2**
(1998) 373.
- [16] F. del Aguila, A. Culatti, R. Munoz-Tapia, M. Perez-Victoria, Phys. Lett. B **419**
(1998) 263; F. del Aguila and M. Perez-Victoria, Acta Phys. Polon. B **28** (1997)
2279.
- [17] T. Hahn and M. Perez-Victoria, Comput. Phys. Commun. **118** (1999) 153; T. Hahn
and M. Rauch, Nucl. Phys. Proc. Suppl. **157** (2006) 236; G. J. van Oldenborgh,
Comput. Phys. Commun. **66** (1991) 1.
- [18] A. Denner and S. Dittmaier, Nucl. Phys. B **658** (2003) 175.
- [19] S. Schael *et al.* [ALEPH Collaboration], Eur. Phys. J. C **47**, 547 (2006).

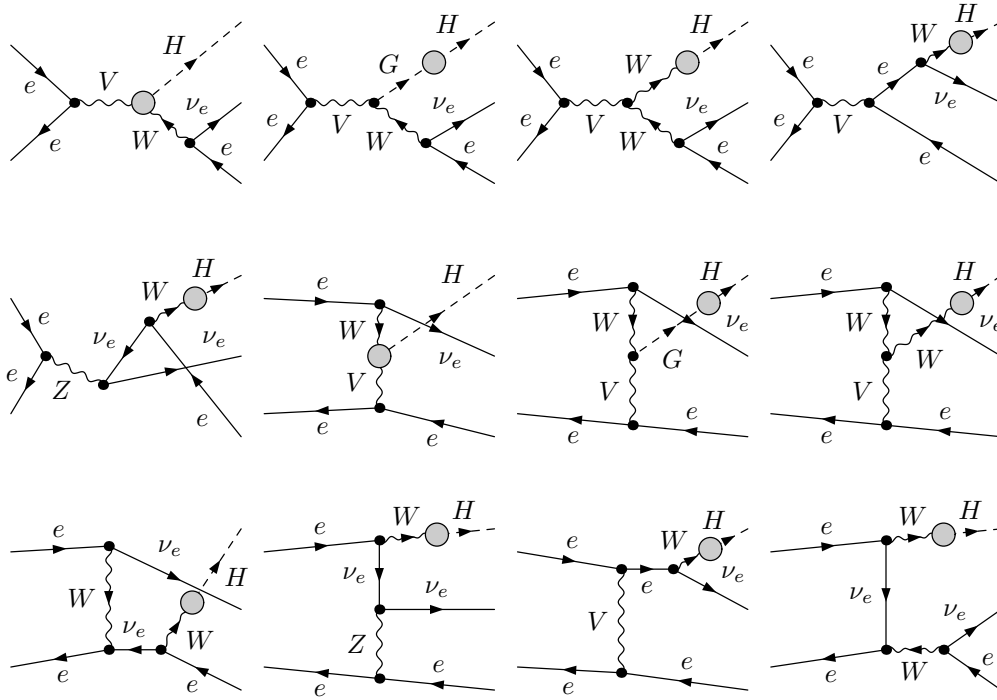


Figure 1: Feynman graphs for $e^+e^- \rightarrow e^+\nu_e H^-$ with insertions of self-energy and $\gamma W^+ H^-$ and $ZW^+ H^-$ vertex corrections. The counter-term graphs have exactly the same structure, with the loop-insertion replaced by the appropriate counter-term. Here $V = \gamma, Z$.

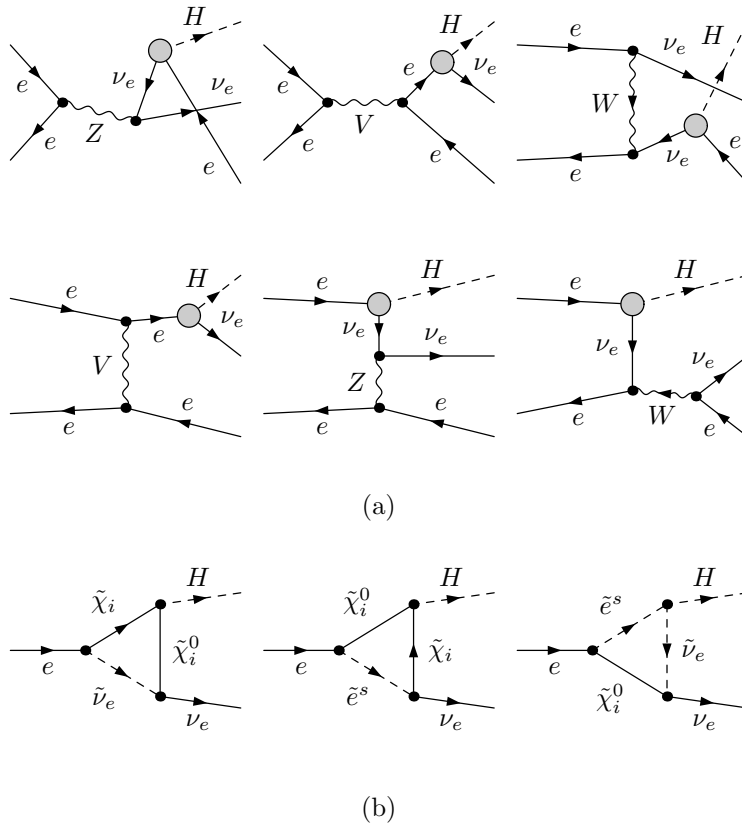


Figure 2: (a) Non-vanishing Feynman graphs for $e^+e^- \rightarrow e^+\nu_e H^-$ with $e^\pm\nu_e H^\mp$ Yukawa coupling insertions. (b) Superpartner corrections to the $e^\pm\nu_e H^\mp$ Yukawa coupling which do not vanish for $m_e = 0$. Here $V = \gamma, Z$.

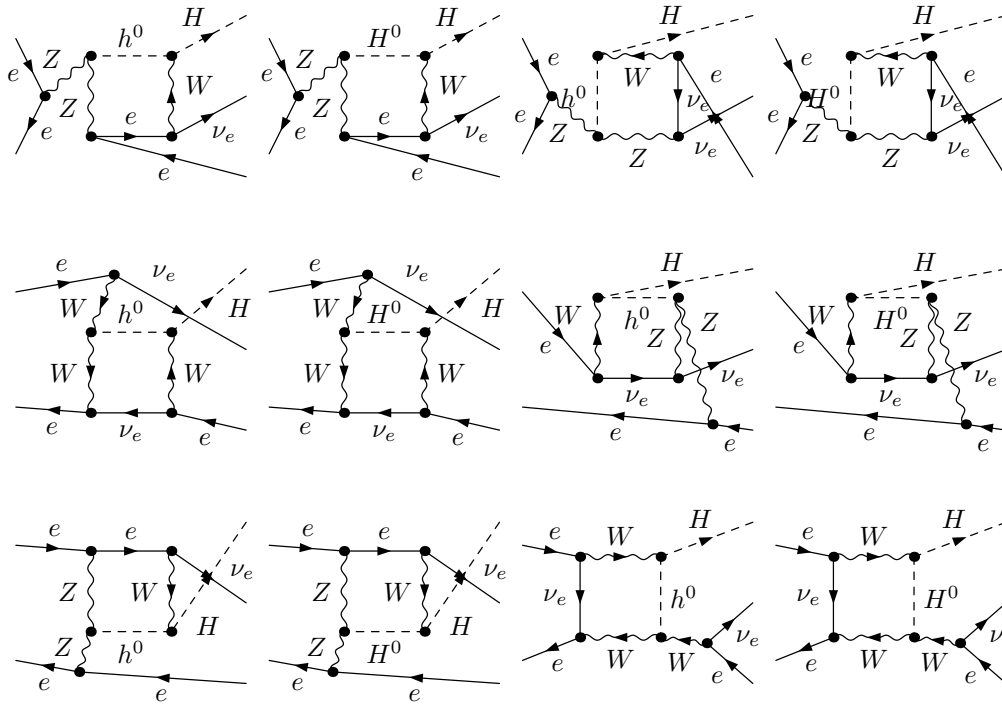


Figure 3: Box-type Feynman graphs for $e^+e^- \rightarrow e^+\nu_e H^-$ in the THDM.

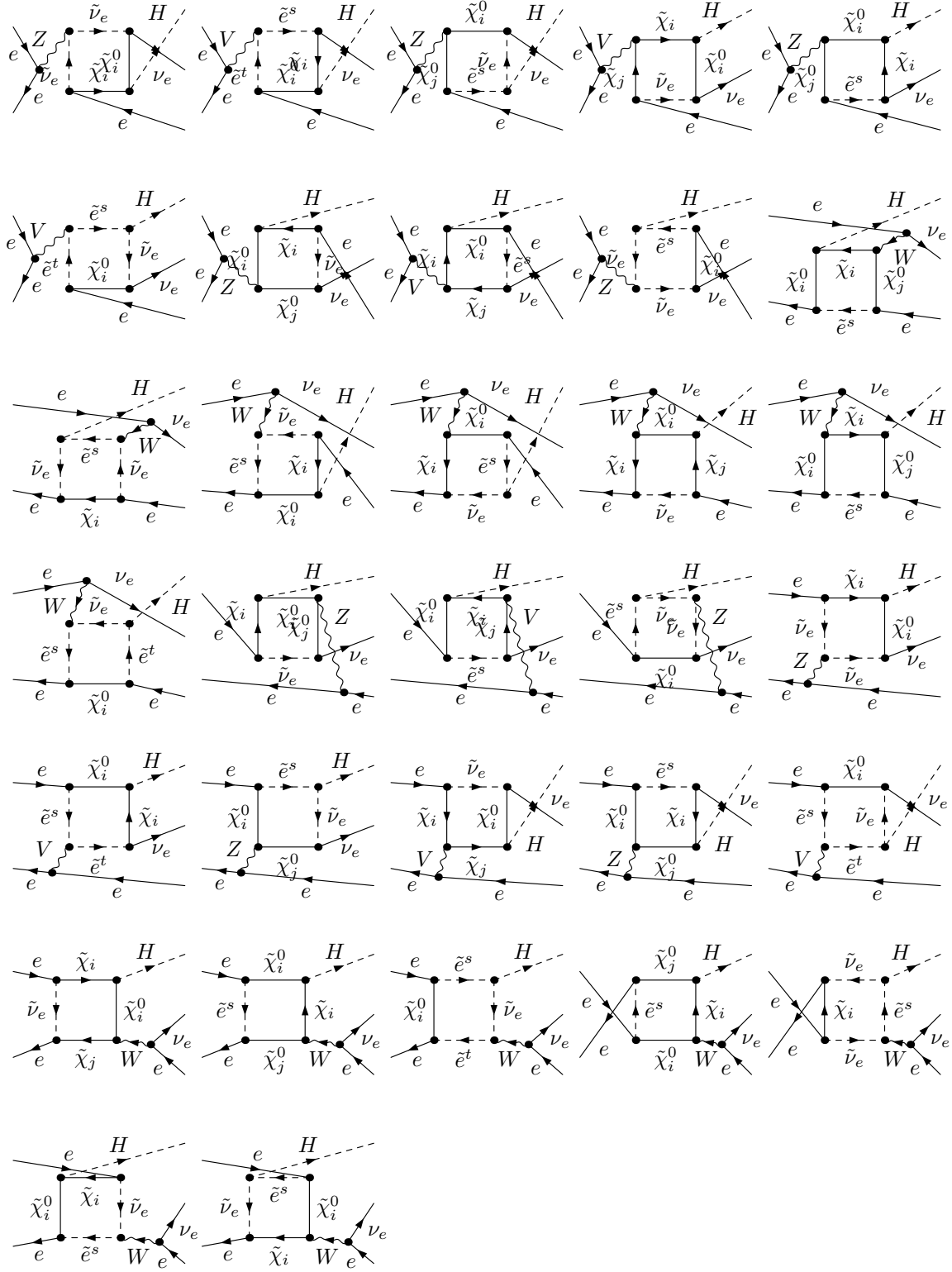


Figure 4: Box-type Feynman graphs for $e^+e^- \rightarrow e^+\nu_e H^-$ with virtual superpartners in the MSSM. Here $V = \gamma, Z$.

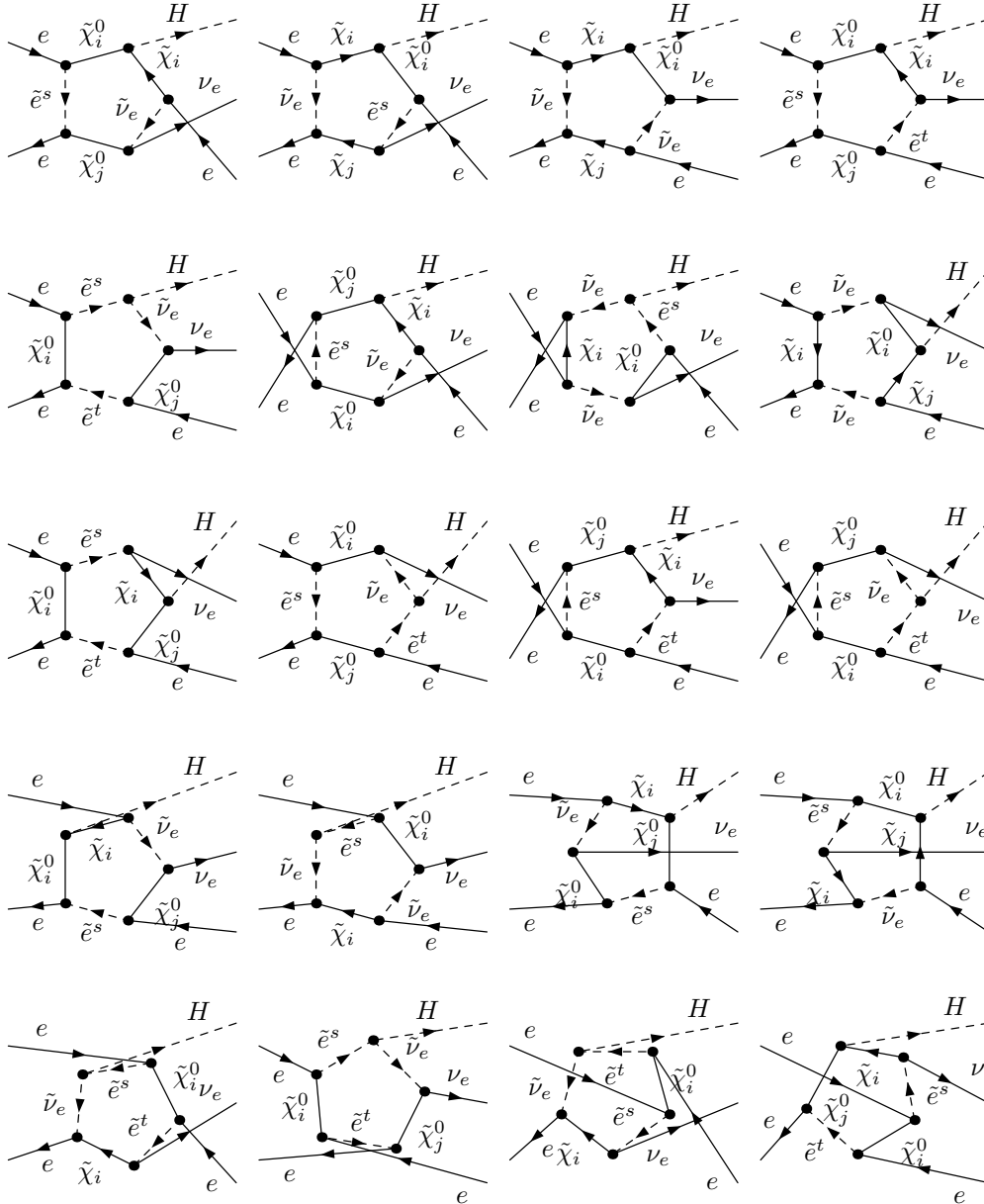


Figure 5: Pentagon-type Feynman graphs for $e^+e^- \rightarrow e^+\nu_e H^-$ in the MSSM.

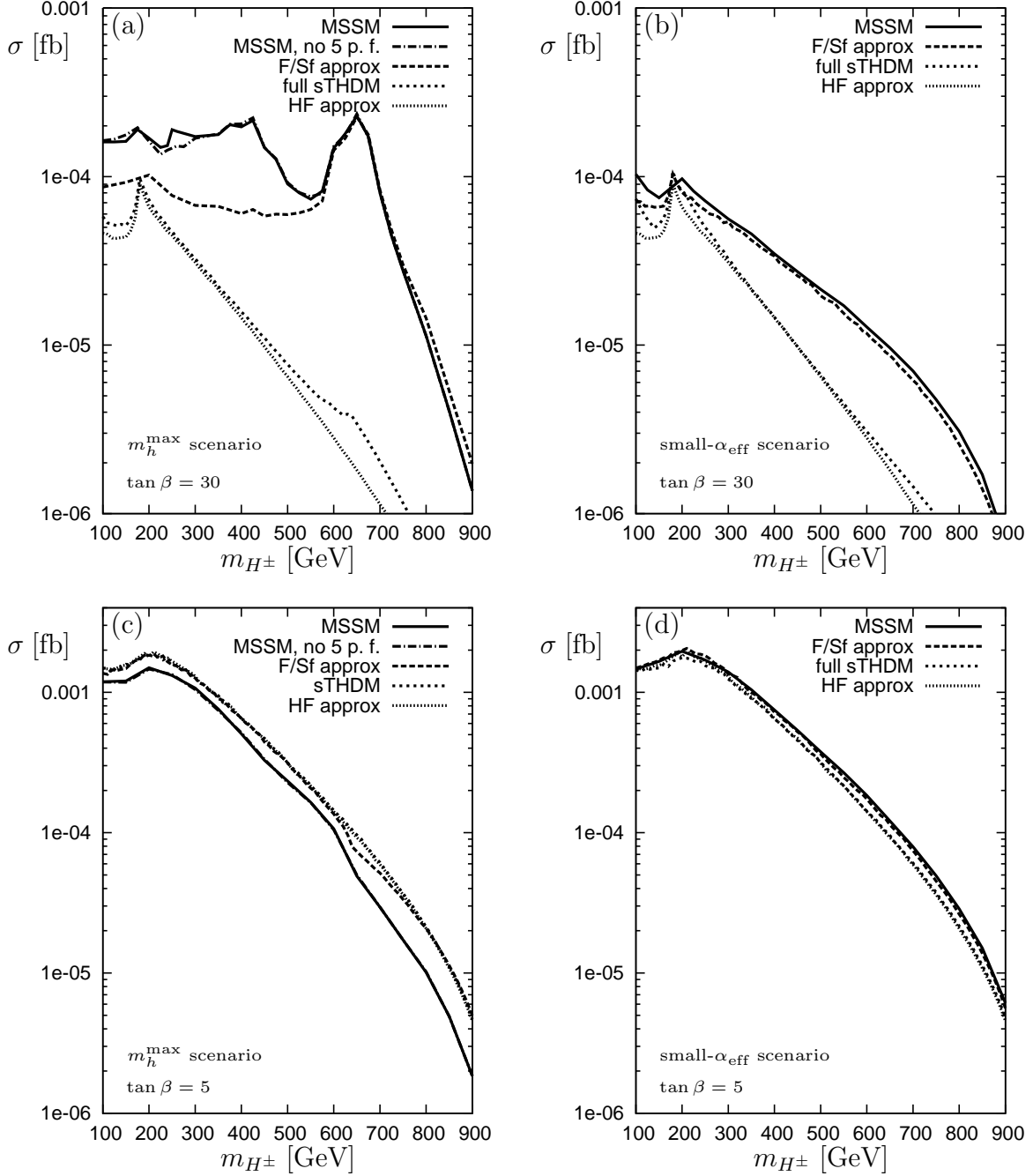


Figure 6: Cross section for the process $e^+e^- \rightarrow (H^+e^-\bar{\nu}_e, H^-e^+\nu_e)$ as a function of a charged Higgs mass m_{H^\pm} for the $m_h^{\max}(400)$ scenario and the small- α_{eff} scenario for $\tan \beta = 30$ and 5. Curves are shown for the full MSSM (solid lines), the Fermion/Sfermion approximation (long dashed lines), the full sTHDM (dashed lines), and the Heavy Fermion approximation (dotted lines). For the $m_h^{\max}(400)$ scenario we also show the MSSM result without pentagons (dot-dashed lines).

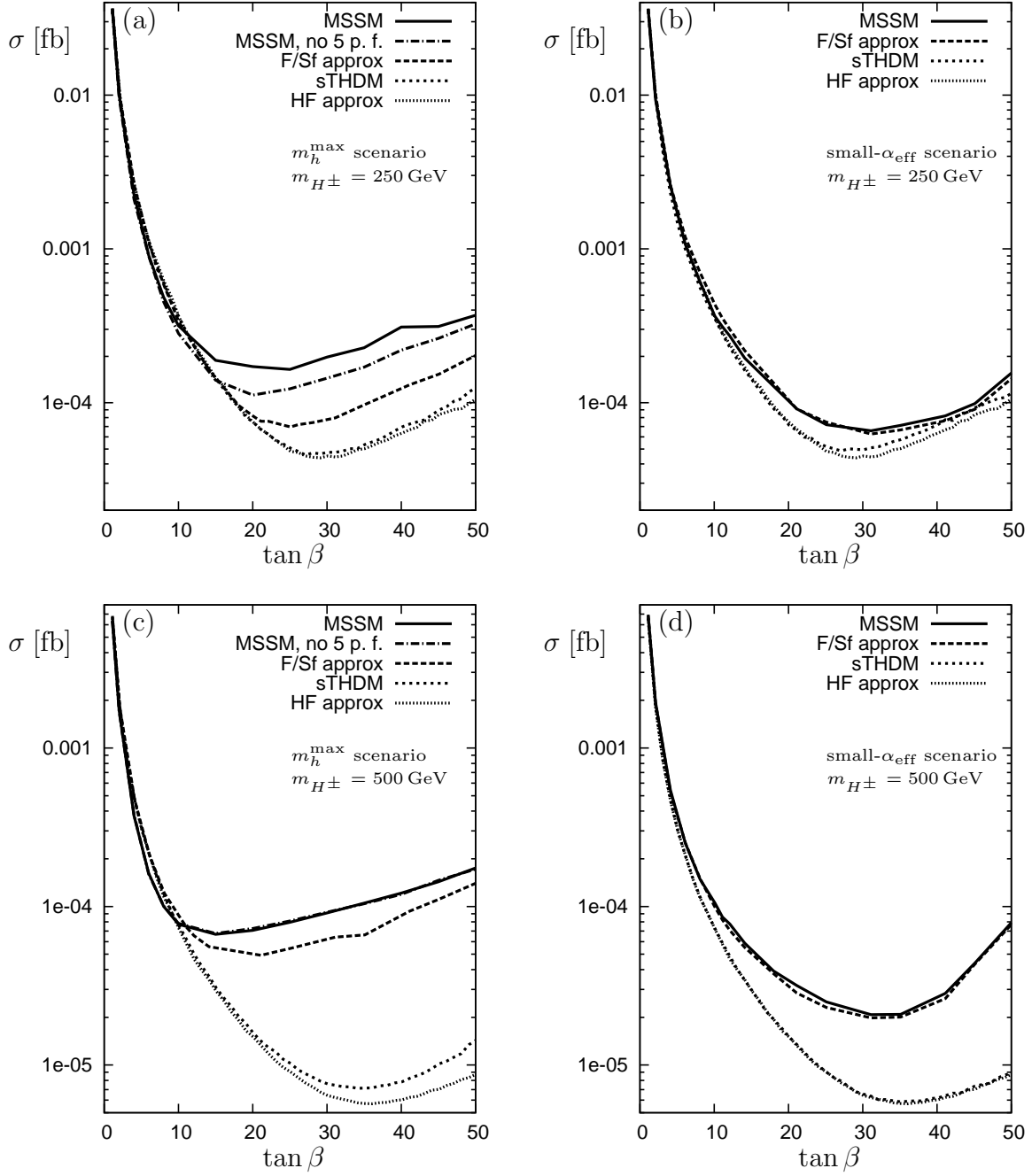


Figure 7: Cross section for the process $e^+e^- \rightarrow (H^+e^-\bar{\nu}_e, H^-e^+\nu_e)$ as a function of $\tan \beta$ for the $m_h^{\max}(400)$ scenario and the small- α_{eff} scenario for $m_{H^\pm} = 250$ GeV and 500 GeV. Curves are shown for the full MSSM (solid lines), the Fermion/Sfermion approximation (long dashed lines), the full sTHDM (dashed lines), and the Heavy Fermion approximation (dotted lines). For the $m_h^{\max}(400)$ scenario we also show the MSSM result without pentagons (dot-dashed lines).

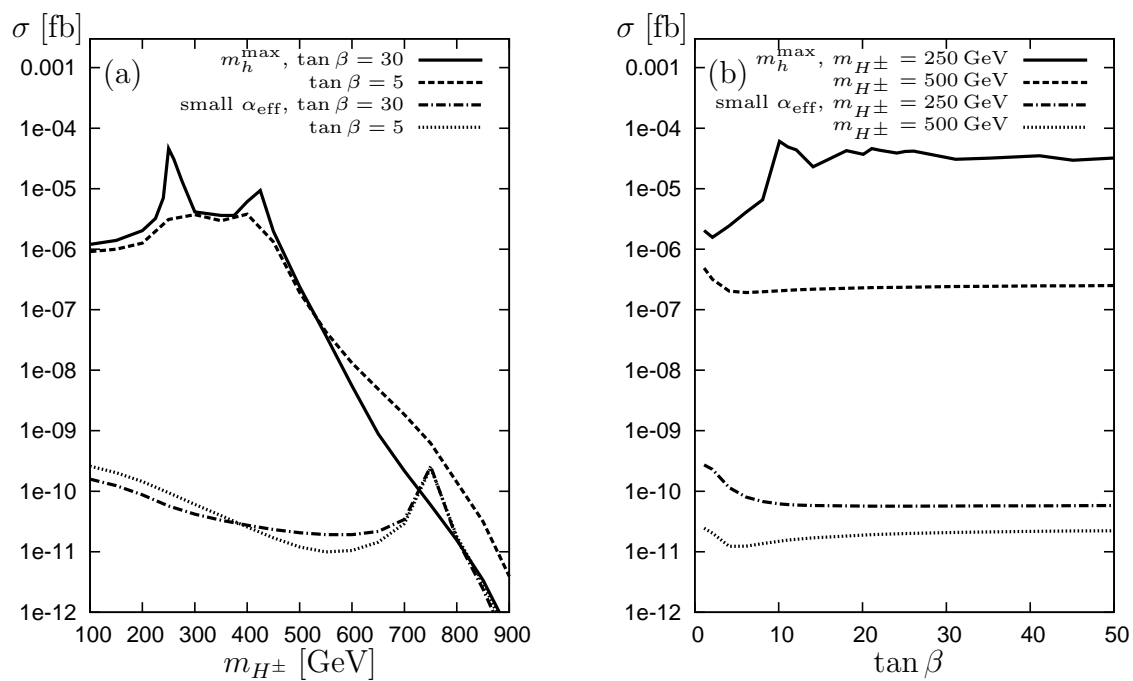


Figure 8: Cross section value for the process $e^+e^- \rightarrow (H^+e^-\bar{\nu}_e, H^-e^+\nu_e)$ resulting from only using the pentagon graphs in the amplitude as a function of (a) m_{H^\pm} and (b) $\tan \beta$. Shown are results for the $m_h^{\max}(400)$ scenario (solid and dashed lines) and the small- α_{eff} scenario (dot-dashed and dotted).